

## Chapter 3

# Organic Light-Emitting Diodes with Field-Effect Electron Transport

In standard OLEDs the total thickness of the organic layers is generally limited to 80 to 100 nm to obtain efficient charge transport at reasonable driving voltages [244]. Consequently, light is generated very close (within ca. 50 nm) to the metallic cathode and the proximity of the metal electrode induces severe optical absorption losses if the OLED is used as a waveguide. In order to sufficiently reduce these optical losses a possible strategy is to increase the thickness of the organic layers [84, 215]. The low carrier mobilities in organic semiconductors [31, 32], however, prevent an arbitrary increase of this thickness and other techniques, such as the use of transparent conductive oxides [96, 217, 218] and careful optical design [182, 219], are necessary to minimize the losses induced by the electrodes.

In LEOFET devices on the other hand, charge carriers have a field-effect mobility which is typically several orders of magnitude higher than the charge carrier mobility in conventional OLEDs [46], and depending on the type of LEOFET, the light-emission zone can be located at a relatively large distance from the metallic source and drain electrodes [65, 66]. Furthermore, high current densities have been reported for LEOFET devices [63, 69, 75]. However, to obtain these properties, three different electrodes must be used, namely the source, the drain and the gate. In addition, most organic field-effect materials demonstrate rather weak photoluminescence and vice versa, most organic light-emitting materials have poor field-effect performance [57]. Indeed, a high carrier mobility, as needed in transistors, is favored by a tight intermolecular  $\pi$  stacking. Examples are pentacene [245] and region-regular P3HT [246]. However, the photoluminescence yield is usually low in such materials with strong intermolecular coupling. Conversely, materials with high photoluminescence quantum yield, e.g. PPVs [247] are usually characterized by a low intermolecular coupling, and thus limited hopping transport between molecules [248]. Therefore, it would be desirable to form a more elaborated heterojunction consisting of charge transport layers and a light-emitting layer, which can be optimized separately [249]. Such heterojunction concepts are commonly used in high-performance OLEDs [33, 34]. In LEOFET device architectures, however, this approach is difficult to apply.

In this chapter, a novel two-electrode light-emitting device structure is proposed. The device is a hybrid structure between a diode and a field-effect transistor. Com-

pared to conventional OLEDs, the cathode is displaced one to several micrometers from the light-emission zone. As the light emission zone is not covered by metal, the device can be used for top emission or even as waveguide. The micrometer-sized distance between the cathode and the active region can be bridged by electrons with an enhanced field-effect mobility. Owing to this high charge carrier mobility, large current densities are possible. The external quantum efficiency at these high current densities is as high as that of conventional OLEDs using the same materials. In contrast to organic light-emitting field-effect transistors, only two electrodes are used. Moreover, light-emission in the novel device structure always occurs at a fixed position, irrespective of the applied bias, in contrast to LEOFETs where the emission zone can move within the channel by varying the bias conditions [65–67]. The first section of this chapter describes the technology and the materials used to fabricate the device. Next, the device operation and the device performance are discussed. The electrical characteristics as well as the opto-electronic performance are studied. Suggestions for further improvement of the device performance are given in the last section of this chapter. The content of this chapter is published in [250, 251].

### 3.1 Device Fabrication

The schematic architecture of the device is illustrated in Fig. 3.1. The device is fabricated on top of an ITO-coated glass substrate and comprises an organic hole-transporting layer (HTL), an organic light-emitting layer and an organic electron-transporting layer (ETL). Prior to the deposition of these organic layers, an insulating layer of 100 nm  $\text{SiO}_2$  is deposited by sputtering. Trenches are selectively wet-etched through the  $\text{SiO}_2$ , to be able to contact the ITO layer. ITO serves as the hole-injecting electrode in the device. The cathode is formed by a thin layer of 0.8 nm lithium fluoride (LiF) followed by the deposition of 100 nm aluminum (Al).

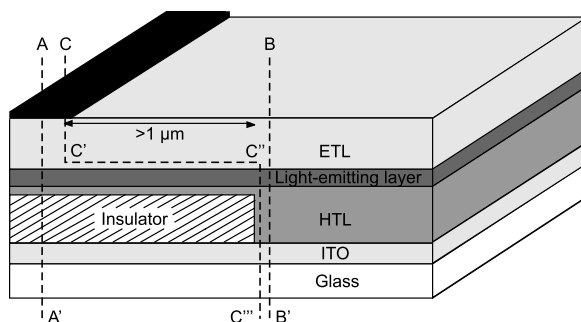


**Fig. 3.1** Schematic architecture of the organic light-emitting diode with field-effect electron transport. The device comprises an organic hole-transporting layer (HTL), an organic electron-transporting layer (ETL) and an organic light-emitting layer. The dashed lines AA', BB' and CC'C''C''' indicate three different sections. (© Wiley-VCH Verlag GmbH & Co. KGaA. Reproduced with permission)

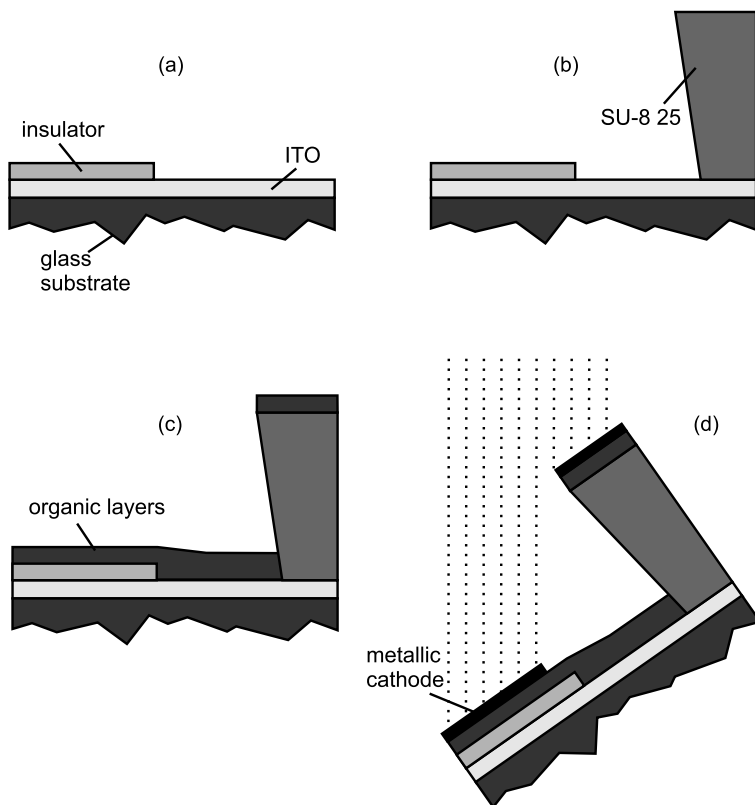


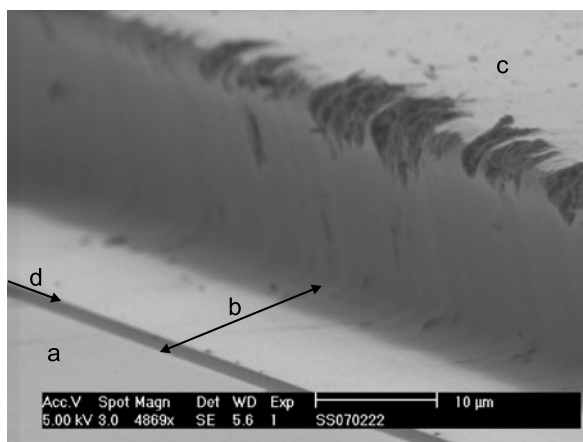
**Fig. 3.2** Schematic depiction of the processing sequence for the fabrication of the light-emitting field-effect device structure: (a) situation before creation of the integrated shadow mask, (b) deposition of the integrated shadow mask, (c) deposition of the organic layers, and (d) deposition of the metallic cathode with the substrate mounted on a triangular sample holder. During this deposition process, the atomic flux is at a  $45^\circ$  angle with respect to the substrate. (© Wiley-VCH Verlag GmbH & Co. KGaA. Reproduced with permission)

This cathode is not positioned vertically above the ITO anode in the trench in the  $\text{SiO}_2$  insulator, but it is located fully above the insulator, as shown in Fig. 3.1. The distance between the metallic top electrode and the insulator edge is one to several microns. Accurate alignment of the metallic cathode is obtained by using an integrated shadow mask technique [252] and angled deposition of the LiF/Al layer (Fig. 3.2).

The integrated shadow mask is realized by patterning a  $20\text{-}\mu\text{m}$  thick negative photoresist SU-8 25 (MicroChem Corp., used as received). This layer is resistant to solvents, acids and bases and has excellent thermal stability. The different organic layers are deposited after application and patterning of the SU-8 25 resist. Subsequently, the sample is mounted on a triangular sample holder and loaded in the ultra-high vacuum system for cathode evaporation. During this deposition, the flux is at a  $45^\circ$  angle with respect to the substrate. The SU-8 25 profile thus creates

**Fig. 3.3** SEM image of the device structure: (a) metallic cathode, (b) shadowed region where no metal is deposited, (c) the 20- $\mu\text{m}$  thick SU-8 25 layer and (d) arrow indicating the insulator edge.

(© Wiley-VCH Verlag GmbH & Co. KGaA. Reproduced with permission)



a shadowed region with a span similar to the thickness of the SU-8 25, so that the substrate is only partially covered with the metal. Figure 3.3 shows a SEM image of the device structure. The shadowed region where no metal is deposited can be recognized. It can also be verified that the walls of the SU-8 25 layer are slightly re-entrant, which is typical for negative photoresists.

PTAA [253] is selected as the hole-transporting material to fabricate the device. This material can be deposited by spincoating, which results in a film with a smooth top surface, favorable for the growth of an additional layer. The bulk hole mobility of PTAA is approximately  $10^{-2} \text{ cm}^2/\text{Vs}$  [253]. For the active light-emitting layer 20 nm  $\text{Alq}_3$  doped with 2% of  $\text{DCM}_2$  is chosen.  $\text{DCM}_2$  is a well-known red light-emitting fluorescent dye used in OLEDs [254], with a photoluminescence quantum yield of about 40% [41]. The organic layer stack is finalized by the deposition of an organic electron-transporting layer. This electron-transporting material is selected according to two criteria which are important in our device architecture. First, the organic electron-transporting material should have a high electron field-effect mobility since this mobility determines the performance. Numerical simulations indicate that the electron mobility is much more critical for the device performance than the mobility of the holes. Second, as electron transport is intended to occur at the heterojunction between the electron-transporting layer and the light-emitting layer, the LUMO of the electron-transporting material should be slightly lower than the LUMO of  $\text{Alq}_3$  and  $\text{DCM}_2$ .  $\text{PTCDI-C}_{13}\text{H}_{27}$  satisfies these two conditions and therefore it is used as the electron-transporting material. Typically, 50 nm  $\text{PTCDI-C}_{13}\text{H}_{27}$  is deposited at a deposition rate of  $0.5 \text{ \AA}/\text{s}$ , while the substrate is kept at room temperature. Gundlach *et al.* reported a field-effect mobility of about  $0.6 \text{ cm}^2/\text{Vs}$  for  $\text{PTCDI-C}_{13}\text{H}_{27}$  using chromium (Cr) top-contacts [255]. A mobility of  $0.28 \text{ cm}^2/\text{Vs}$  was obtained using  $\text{LiF}/\text{Al}$  top-contacts. Even higher field-effect mobilities can be achieved by annealing after fabrication [256]. The molecular structures and the energy levels of the HOMO and the LUMO of PTAA,  $\text{Alq}_3$ ,  $\text{DCM}_2$  and  $\text{PTCDI-C}_{13}\text{H}_{27}$  can be found in Chap. 2 (Sect. 2.1.1).

## 3.2 Device Operation

To explain the device operation we draw in Fig. 3.4 the band diagrams through sections AA', BB' and CC'C''C''' of Fig. 3.1 for the device in forward bias, i.e. for a positive anode-to-cathode bias. Under these conditions electrons are injected from the cathode into PTCDI-C<sub>13</sub>H<sub>27</sub> at cross-section AA'. The semiconductor PTAA and the light-emitting layer Alq<sub>3</sub>:DCM<sub>2</sub> on top of the SiO<sub>2</sub> (cross-section AA') are depleted of holes. As will be confirmed further, the LUMO offset at the interface between Alq<sub>3</sub> and PTCDI-C<sub>13</sub>H<sub>27</sub> prohibits electron injection from PTCDI-C<sub>13</sub>H<sub>27</sub> into Alq<sub>3</sub> in the cross-section AA'. As a result, the depleted PTAA layer and Alq<sub>3</sub>:DCM<sub>2</sub> layer on top of the SiO<sub>2</sub> insulator behave as a dielectric layer in series to the SiO<sub>2</sub> insulator, and an electron accumulation layer is formed in the PTCDI-C<sub>13</sub>H<sub>27</sub> at the interface with Alq<sub>3</sub>:DCM<sub>2</sub>. These electrons are transported laterally by the electric field from the cathode towards the SiO<sub>2</sub> edge (from C' to C''). The field-effect mobility of these charge carriers is larger than the charge carrier mobility in a conventional OLED, making transport over several microns possible. Near the insulator edge, at position C'', electrons are injected into the Alq<sub>3</sub>:DCM<sub>2</sub> layer, where they recombine with holes, injected from the ITO and transported vertically through the PTAA (see cross-section BB' in Fig. 3.4). The electron injection at position C'' into Alq<sub>3</sub> is enabled by an enhanced vertical electric field at that position.

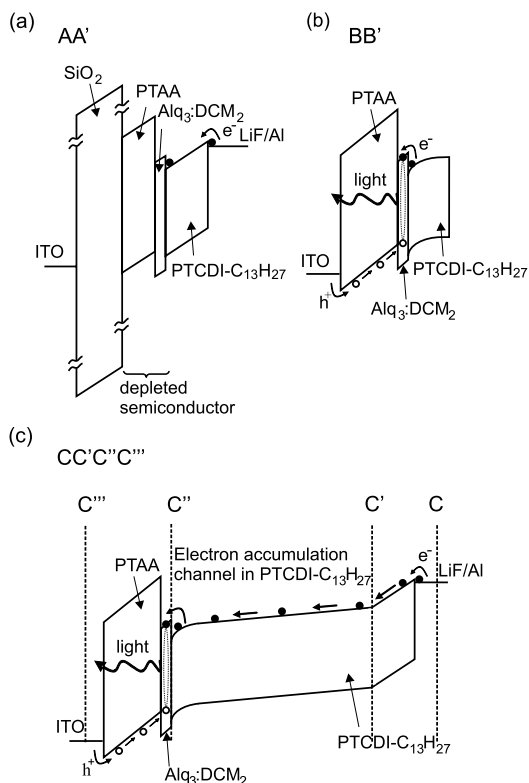
**Fig. 3.4** Band diagrams for the device under forward bias conditions through different sections of Fig. 3.1:

(a) cross-section AA',

(b) cross-section BB' and

(c) section CC'C''C'''.

(© Wiley-VCH Verlag GmbH & Co. KGaA. Reproduced with permission)



The enhancement of the vertical field at  $C''$  has two causes: first, the vertical and lateral electric fields in the channel (section  $C'C''$ ) collapse into only a vertical field at position  $C''$ ; furthermore, the presence of a space charge of holes in PTAA increases the vertical electrical field that attracts electrons to be injected in the  $\text{Alq}_3:\text{DCM}_2$  layer. This latter behavior is similar to the enhanced hole injection as a result of a space charge of electrons at the anode of OLEDs reported by Van Woudenberg *et al.* [257]. Exciton formation occurs and radiative relaxation of these excitons to the ground state results in light-emission near the  $\text{SiO}_2$  edge, at a micrometer-size distance from the metallic contact. In this way, this heterojunction device allows to minimize optical losses at the metal cathode. The vicinity of the ITO bottom-contact is of minor importance with respect to absorption losses because it has been shown that thin transparent ITO layers have low optical losses in the 550–750 nm spectral range [184]. Note that since the potential near the insulator edge is floating and since there is no electron confinement in the lateral direction (the electrons are not hindered by an interface), the electron and hole current in the device are always balanced.

We have confirmed this view of the device operation by measuring the characteristics of several control devices. Control transistors comprising the stacks PTAA/PTCDI- $\text{C}_{13}\text{H}_{27}$  and PTAA/ $\text{Alq}_3:\text{DCM}_2$ /PTCDI- $\text{C}_{13}\text{H}_{27}$  have been fabricated on doped  $n^{++}$ -Si wafers with a 100-nm thick thermally grown  $\text{SiO}_2$  layer (serving as the OTFT gate dielectric). LiF/Al was used as source and drain top electrodes. For the PTAA/PTCDI- $\text{C}_{13}\text{H}_{27}$  transistor, a field-effect mobility for electrons in PTCDI- $\text{C}_{13}\text{H}_{27}$  at the heterojunction interface with PTAA of  $0.2 \text{ cm}^2/\text{Vs}$  is extracted. It is striking that the hole-transporting organic semiconductor PTAA provides a good growth surface for the electron-conducting PTCDI- $\text{C}_{13}\text{H}_{27}$ , and that the hetero-interface is appropriate for electron transport. This can be attributed to the smooth top surface of PTAA and the formation of a high-quality interface free of electron traps. We infer the latter from the observation that the electron mobility in PTCDI- $\text{C}_{13}\text{H}_{27}$  transistors on PTAA-coated  $\text{SiO}_2$  is the same as the one we measured in control transistors that have a gate dielectric consisting of  $\text{SiO}_2$  coated with  $\text{P}\alpha\text{MS}$ , known to provide a high-quality, electron-trap free surface [258] that allows good electron transport [259].

Upon inserting  $\text{Alq}_3:\text{DCM}_2$  between PTAA and PTCDI- $\text{C}_{13}\text{H}_{27}$ , the effective saturation field-effect electron mobility drops to  $0.08 \text{ cm}^2/\text{Vs}$ . The output and transfer characteristics of this transistor are shown in Fig. 3.5. We correlate the reduction in mobility to the different growth of PTCDI- $\text{C}_{13}\text{H}_{27}$  on  $\text{Alq}_3:\text{DCM}_2$  as compared to growth on PTAA. Figures 3.6(a) and (b) show the PTCDI- $\text{C}_{13}\text{H}_{27}$  morphology on, respectively, PTAA and PTAA/ $\text{Alq}_3:\text{DCM}_2$ . PTCDI- $\text{C}_{13}\text{H}_{27}$  deposited on PTAA/ $\text{Alq}_3:\text{DCM}_2$  reveals a much rougher growth than PTCDI- $\text{C}_{13}\text{H}_{27}$  grown on top of PTAA; this correlates with the lower field-effect mobility. The rms roughness of the layer is increased from 6.7 nm to 10.7 nm upon inserting an  $\text{Alq}_3:\text{DCM}_2$  layer. As both substrates (PTAA and PTAA/ $\text{Alq}_3:\text{DCM}_2$ ) are morphologically similar, being amorphous flat surfaces with the same rms roughness of 0.4 nm, the difference in growth of PTCDI- $\text{C}_{13}\text{H}_{27}$  originates from the interfacial energy differences between, respectively, PTCDI- $\text{C}_{13}\text{H}_{27}$  and PTAA and PTCDI- $\text{C}_{13}\text{H}_{27}$  and  $\text{Alq}_3:\text{DCM}_2$ .

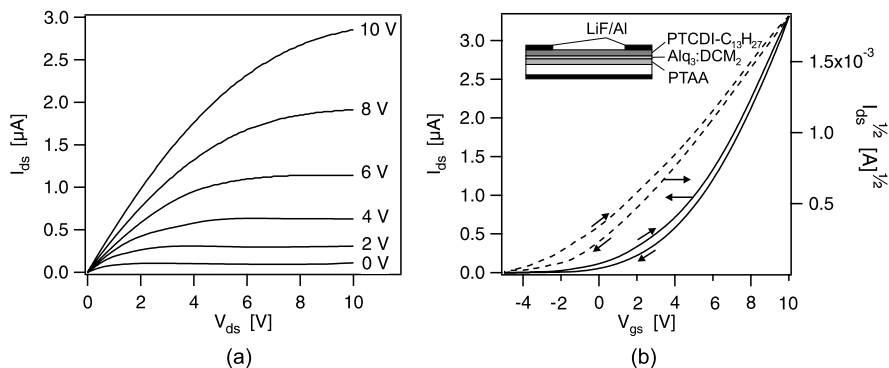


**Fig. 3.5** Electrical characteristics of a top-contact transistor comprising PTAA/Alq<sub>3</sub>:DCM<sub>2</sub>/PTCDI-C<sub>13</sub>H<sub>27</sub> as the organic layers ( $W/L = 2000/50$ ). (a) Output characteristics for various  $V_{gs}$ , and (b) transfer characteristics of the same transistor. A saturation mobility of  $0.08 \text{ cm}^2/\text{Vs}$  and a threshold voltage of  $\sim 0 \text{ V}$  are extracted for this device. (© Wiley-VCH Verlag GmbH & Co. KGaA. Reproduced with permission)

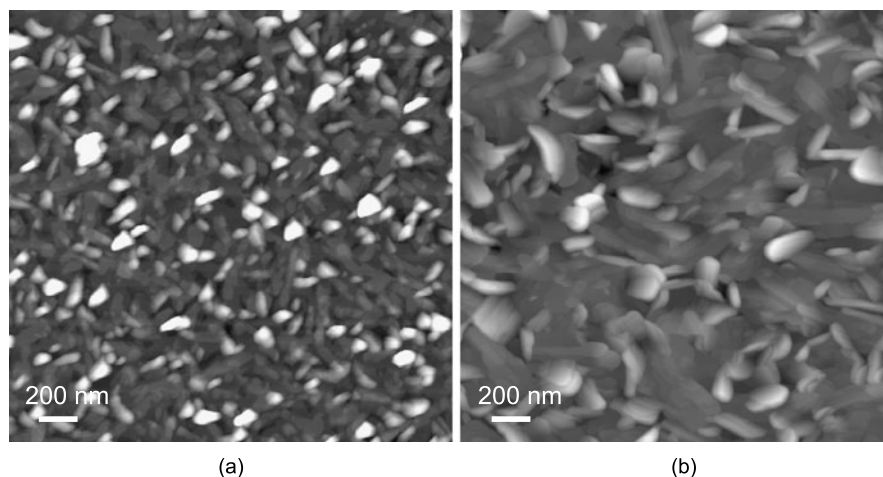


**Fig. 3.6**  $2 \mu\text{m} \times 2 \mu\text{m}$  atomic force microscopy (AFM) surface scans of a  $50 \text{ nm}$  thick PTCDI-C<sub>13</sub>H<sub>27</sub> layer on top of (a) PTAA and (b) PTAA/Alq<sub>3</sub>:DCM<sub>2</sub>. On PTAA/Alq<sub>3</sub>:DCM<sub>2</sub> a higher surface roughness is measured: the rms roughness is  $10.7 \text{ nm}$  for PTCDI-C<sub>13</sub>H<sub>27</sub> on PTAA/Alq<sub>3</sub>:DCM<sub>2</sub> versus  $6.7 \text{ nm}$  for PTCDI-C<sub>13</sub>H<sub>27</sub> grown on PTAA. (© Wiley-VCH Verlag GmbH & Co. KGaA. Reproduced with permission)

Additionally, a control transistor was fabricated comprising PTAA/Alq<sub>3</sub>:DCM<sub>2</sub> as the organic layers, to verify whether Alq<sub>3</sub>:DCM<sub>2</sub> could not be used as the electron-transport layer instead of PTCDI-C<sub>13</sub>H<sub>27</sub>. No field-effect transport of electrons could be observed in this structure. The non-planar molecular structure of Alq<sub>3</sub> apparently prohibits efficient lateral electron transport. This control experiment also proves that electron transport in the transistor comprising the organic

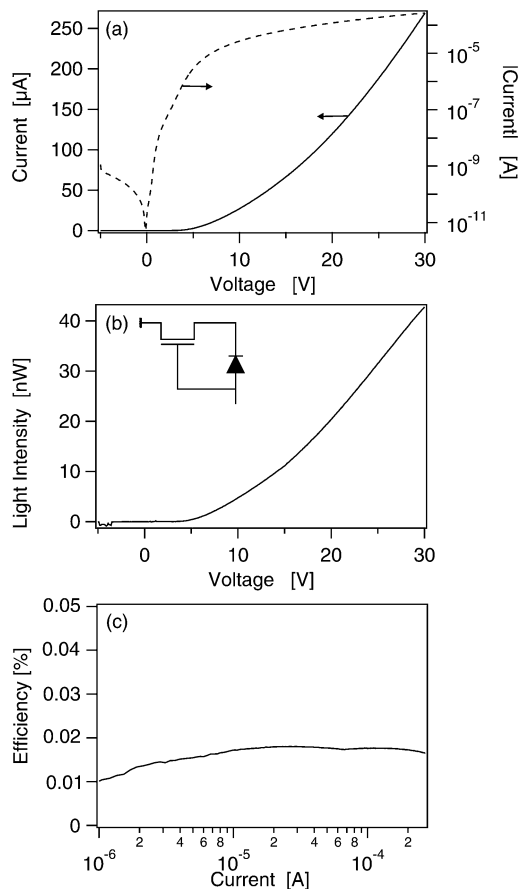
stack PTAA/Alq<sub>3</sub>:DCM<sub>2</sub>/PTCDI-C<sub>13</sub>H<sub>27</sub> and in our novel device structure (between position C' and C'' in Fig. 3.1) indeed occurs in the PTCDI-C<sub>13</sub>H<sub>27</sub> and not in Alq<sub>3</sub>:DCM<sub>2</sub>.

### 3.3 Device Performance

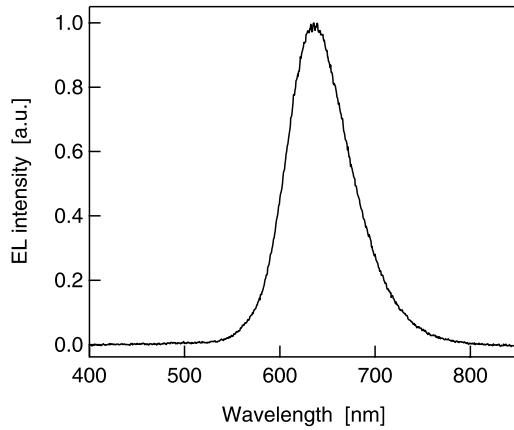
#### 3.3.1 Optical and Electrical Characterization

Figure 3.7(a) displays the experimentally measured electrical characteristics of a light-emitting device constructed by using the architecture depicted in Fig. 3.1. The device has a width of 1 mm and was measured in an inert N<sub>2</sub> atmosphere immediately after evaporation. The metallic cathode of the device is displaced by 3.5 μm with respect to the insulator edge. Under forward bias, the current increases with increasing voltage. The electrical characteristics can be explained by the equivalent

**Fig. 3.7** Experimentally measured characteristics of the light-emitting diode with field-effect electron transport. This device has a width of 1 mm and a distance between the top electrode and the insulator edge of 3.5 μm. (a) Current-voltage characteristics, (b) corresponding light output. *Inset*: equivalent circuit of the device, and (c) external quantum efficiency as a function of the current. (© Wiley-VCH Verlag GmbH & Co. KGaA. Reproduced with permission)



**Fig. 3.8** Normalized electroluminescence spectrum of the light-emitting diode with field-effect electron transport. The spectrum corresponds to DCM<sub>2</sub> emission with a maximum positioned at wavelength  $\lambda = 636$  nm. (© Wiley-VCH Verlag GmbH & Co. KGaA. Reproduced with permission)



circuit shown as inset in Fig. 3.7(b). This equivalent circuit consists of an n-type transistor having a diode between the gate and the drain.

The device emits red light upon the radiative decay of excitons. The optical output intensity as a function of the applied voltage bias is shown in Fig. 3.7(b). It can be seen that the optical output tracks the current characteristics. The normalized electroluminescence (EL) spectrum of the device is shown in Fig. 3.8. The peak emission wavelength is located at 636 nm and corresponds to DCM<sub>2</sub> emission. Two control experiments allowed to verify that the observed emission indeed originates from DCM<sub>2</sub>. In a first control experiment, we changed the dye from DCM<sub>2</sub> to Btp<sub>2</sub>Ir(acac) [260], a phosphorescent dye with characteristic spectral features that could easily be recognized. In another control experiment, we used undoped Alq<sub>3</sub>; this device emits green light, peaking at 540 nm, as is characteristic for emission from Alq<sub>3</sub>.

In our device structure, the emission zone is well-defined and light-emission always occurs at a fixed position, namely near the edge of the insulator. This position is independent of the applied bias. The left panel of Fig. 3.9 shows a photograph in reflection of a device without biasing. The metal electrode (white reflecting area) and the insulator edge, indicated with an arrow, can be recognized. For this device, the distance between the cathode and the insulator edge is 19  $\mu\text{m}$ . The right panel of Fig. 3.9 is an image in the dark of the optical output when the device is in forward bias. A narrow line of red light appears alongside the edge of the insulator. The light intensity increases with the bias voltage. Despite the narrow emission zone, the red light can easily be observed by the naked eye. The measured width of the emission zone is about 2  $\mu\text{m}$ .

### 3.3.2 Analysis

The experimentally observed behavior is qualitatively confirmed by numerical simulations. A simplified device, comprising a hole-transporting layer (HTL) and a

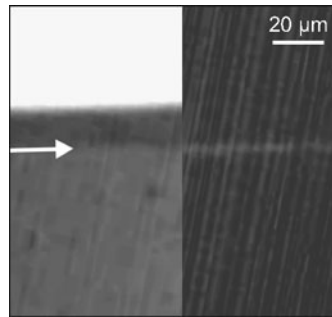


**Fig. 3.9** *Left panel:* Optical microscope reflection image of a device without bias. The *white area* is the reflective metal cathode, the *arrow* indicates the insulator edge. *Right panel:* under forward bias a narrow line of light appears along the insulator edge. The width of the line is estimated to be about 2  $\mu\text{m}$ . (© Wiley-VCH Verlag GmbH & Co. KGaA. Reproduced with permission)

light-emitting electron-transporting layer (ETL), was simulated using the Silvaco ATLAS 2D device simulator. The material parameters used in the simulations are summarized in Table 3.1. For the ETL an electron mobility of  $8 \cdot 10^{-2} \text{ cm}^2/\text{Vs}$  is used, which corresponds to the experimentally measured electron field-effect mobility of PTCDI- $\text{C}_{13}\text{H}_{27}$  in our device. The hole mobility of the ETL is taken to be  $5 \cdot 10^{-4} \text{ cm}^2/\text{Vs}$ . For the HTL on the other hand a hole mobility of  $5 \cdot 10^{-3} \text{ cm}^2/\text{Vs}$  and a negligible electron mobility are taken. The HOMO and LUMO of the ETL and HTL are assumed to be similar to the HOMO and LUMO of, respectively, PTCDI- $\text{C}_{13}\text{H}_{27}$  and PTAA. Typical values for the singlet lifetime ( $\tau$ ) and the exciton diffusion length ( $L_{diff}$ ) are taken from literature [261]. The top contact is assumed to be located at 6  $\mu\text{m}$  from the insulator edge. Figure 3.10(a) illustrates the simulated recombination zone as the result of applying a positive bias to the anode. It can be clearly seen that recombination occurs near the insulator edge, several microns from the metallic contact. The simulated recombination zone has a width of about 2  $\mu\text{m}$ , which is in agreement with the experimental observation. Figure 3.10(b) confirms the presence of an electron accumulation layer at the interface between the HTL and the light-emitting ETL when a positive bias is applied to the anode with respect to the cathode. This electron accumulation region vanishes beyond the insulator edge, as electrons and holes recombine there.

**Table 3.1** Summary of the parameters used in the 2D device simulator

	HTL	Light-emitting ETL
HOMO (eV)	5.1	5.4
LUMO (eV)	1.8	3.4
$\mu_e$ ( $\text{cm}^2/\text{Vs}$ )	$1 \cdot 10^{-7}$	$8 \cdot 10^{-2}$
$\mu_h$ ( $\text{cm}^2/\text{Vs}$ )	$5 \cdot 10^{-3}$	$5 \cdot 10^{-4}$
$L_{diff}$ (nm)		10
$\tau$ (s)		$16 \cdot 10^{-9}$

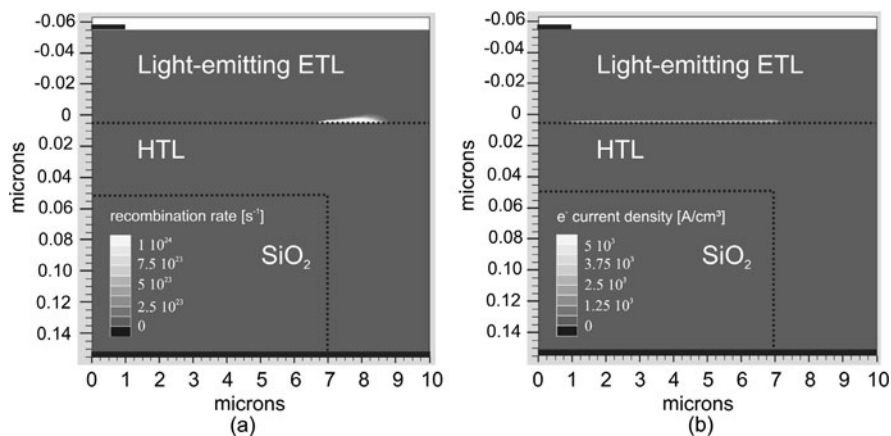


**Fig. 3.10** (a) The simulated recombination rate, and (b) the simulated electron accumulation layer under forward bias. (© Wiley-VCH Verlag GmbH & Co. KGaA. Reproduced with permission)

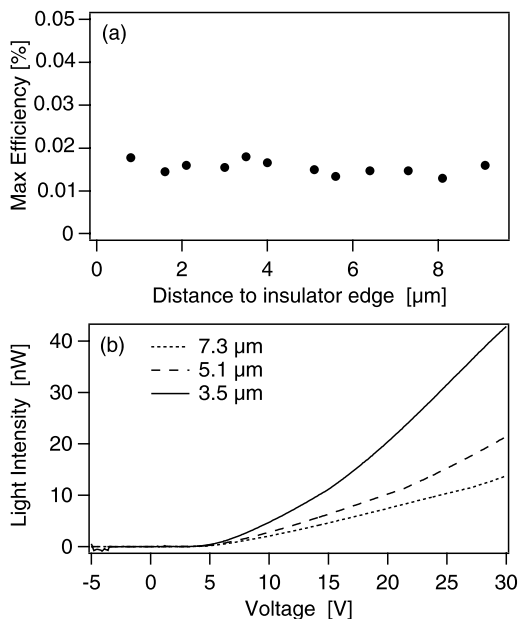
The external quantum efficiency  $\eta_{ext}$  of the fabricated devices is estimated based on luminance, EL spectra and current. The measured maximum  $\eta_{ext}$  of the device is 0.02%, which is similar to that of a light-emitting diode using the same materials. Reference OLEDs with Alq<sub>3</sub>:DCM<sub>2</sub> active layers have been shown with up to 0.5% efficiency [254]. In these reference OLEDs, Alq<sub>3</sub> is used as electron transporting layer, rather than PTCDI-C<sub>13</sub>H<sub>27</sub>. However, Alq<sub>3</sub> cannot be used in our structure because its non-planar molecular structure prohibits efficient electron transport in a thin-film transistor configuration.

By changing the distance between the metallic contact and the insulator edge, the light intensity of the OLED with field-effect electron transport can be tuned. We measured different devices for which the top-contact displacement with respect to the insulator edge is systematically varied from 0.8  $\mu\text{m}$  to 9  $\mu\text{m}$ . In Fig. 3.11(a) the measured maximum  $\eta_{ext}$  of each of these devices is plotted as a function of the distance between the cathode and the insulator edge. As expected, the maximum  $\eta_{ext}$  is constant.

On the other hand, at the average breakdown voltage of the SiO<sub>2</sub> insulator, about 30 V, higher currents are possible in devices with shorter cathode displacement with respect to the insulator edge. As a result, the maximum achievable optical output power and brightness can be higher for smaller distances. This is illustrated in Fig. 3.11(b) which shows the light intensity of three different devices with distances between the metallic cathode and the insulator edge of, respectively, 7.3  $\mu\text{m}$ , 5.1  $\mu\text{m}$  and 3.5  $\mu\text{m}$ .

Taking into account a 2  $\mu\text{m}$  wide emission zone, the maximum hole current density in the device at 30 V is estimated to be 13 A/cm<sup>2</sup>. This current density is much higher than the current density obtained in conventional OLEDs (typically in the order of 10<sup>-2</sup> A/cm<sup>2</sup> at the point of maximum  $\eta_{ext}$ ). The maximum electron current density in the accumulation layer of the light-emitting device is even higher. Assuming a current flow confined to a 5-nm thick electron accumulation layer, which

**Fig. 3.11** (a) The maximum external quantum efficiency  $\eta_{ext}$  as a function of the distance to the insulator edge. Irrespective of the distance, the maximum  $\eta_{ext}$  is constant. (b) Light intensity versus applied voltage of three different devices for which the top-contact displacement with respect to the insulator edge is  $7.3\ \mu\text{m}$  (dotted lines),  $5.1\ \mu\text{m}$  (dashed lines) and  $3.5\ \mu\text{m}$  (full lines), respectively. (© Wiley-VCH Verlag GmbH & Co. KGaA. Reproduced with permission)



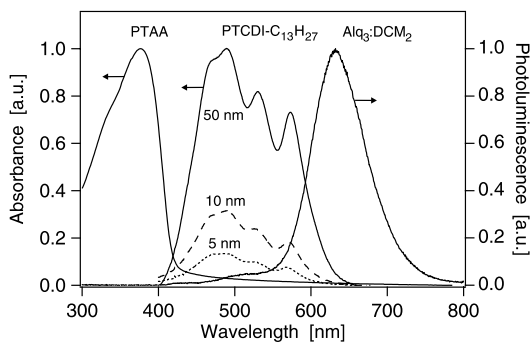
corresponds to approximately two PTCDI- $\text{C}_{13}\text{H}_{27}$  monolayers [256], current densities of  $5400\ \text{A}/\text{cm}^2$  are achieved. This is comparable to the highest current densities achieved in ambipolar organic light-emitting transistors reported to date [63, 75] and can be attributed to the high electron mobility in our device. Figure 3.7(c) shows the measured  $\eta_{ext}$  as a function of the current. Within the experimental error no significant roll-off is observed up to the maximum current.

### 3.4 Improvement of the External Quantum Efficiency

The measured maximum  $\eta_{ext}$  of the fabricated device is 0.02%. This value is rather low compared to reference OLEDs based on  $\text{Alq}_3:\text{DCM}_2$  reported in literature [254]. However, in these reference OLEDs,  $\text{Alq}_3$  is used as the electron-transporting material, instead of PTCDI- $\text{C}_{13}\text{H}_{27}$ , indicating that the presence of PTCDI- $\text{C}_{13}\text{H}_{27}$  might be responsible for the low  $\eta_{ext}$  in our devices.

The low  $\eta_{ext}$  of the devices may have two plausible origins: (i) exciton dissociation at the interface between the  $\text{Alq}_3:\text{DCM}_2$  and the PTCDI- $\text{C}_{13}\text{H}_{27}$  layer; or (ii) re-absorption of the emitted photons by one of the used organic materials. The first of the above mentioned mechanisms would mean that excitons of  $\text{DCM}_2$  (with LUMO of 3.1 eV and HOMO of 5.2 eV) [235] would dissociate to PTCDI- $\text{C}_{13}\text{H}_{27}$  (with LUMO of 3.4 eV) [236] by electron-transfer at the interface between these two materials. To test whether this mechanism is operative, we fabricated devices in which a thin undoped layer of  $\text{Alq}_3$  was inserted between the light-emitting layer and the electron-transporting layer. Such a layer would prohibit the dissociation of

**Fig. 3.12** Normalized photoluminescence spectrum of a thin film of Alq<sub>3</sub> doped with 2% of DCM<sub>2</sub> and absorption spectra of PTAA and PTCDI-C<sub>13</sub>H<sub>27</sub> thin films with different thicknesses: 50 nm (full line), 10 nm (dashed line) and 5 nm (dotted line). (© Wiley-VCH Verlag GmbH & Co. KGaA. Reproduced with permission)

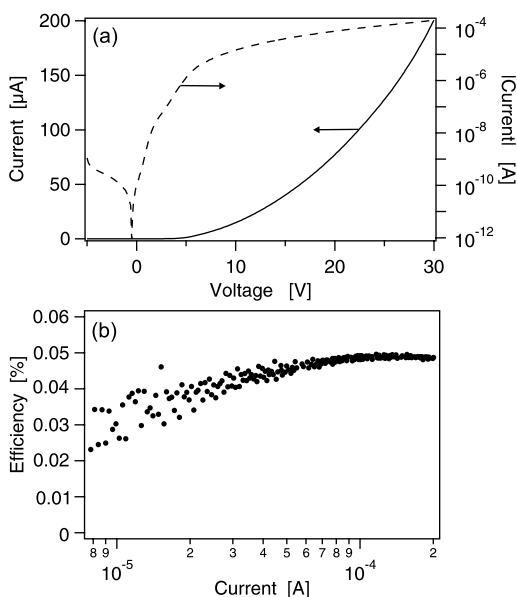


excitons of DCM<sub>2</sub> because the LUMO of Alq<sub>3</sub> (2.8 eV) [235] is higher than the LUMO of DCM<sub>2</sub>. Therefore, if the low  $\eta_{ext}$  is a result of exciton break-up, it would be expected that higher quantum efficiencies could be measured for diodes with an interfacial layer of undoped Alq<sub>3</sub>. Experimentally, we used an interfacial layer of 10 nm of Alq<sub>3</sub>. The  $\eta_{ext}$  remained unaltered. Hence, exciton dissociation cannot be identified as the origin for the low  $\eta_{ext}$  in PTCDI-C<sub>13</sub>H<sub>27</sub>-based devices. Note that an incomplete recombination of holes and electrons due to an imbalance between the electron and hole current can also not be invoked as the reason for the rather low external quantum efficiency, since the electron and hole current in the device are always balanced.

Another possibility is that photons emitted by DCM<sub>2</sub> are re-absorbed by one of the other organic materials that are used to fabricate the device. In Fig. 3.12, the normalized absorption spectra of PTAA and PTCDI-C<sub>13</sub>H<sub>27</sub> and the normalized photoluminescence spectrum of Alq<sub>3</sub>:DCM<sub>2</sub> are shown. The absorption spectrum of PTAA is clearly blue-shifted with respect to the emission of DCM<sub>2</sub>. The emission spectrum of Alq<sub>3</sub>:DCM<sub>2</sub> and the absorption spectrum of PTCDI-C<sub>13</sub>H<sub>27</sub> on the other hand, display a significant overlap, indicating that photons emitted by DCM<sub>2</sub> will be strongly re-absorbed by PTCDI-C<sub>13</sub>H<sub>27</sub>. A simple way to reduce this overlap is by decreasing the PTCDI-C<sub>13</sub>H<sub>27</sub> layer thickness. In Fig. 3.12 the absorption spectra of very thin (5 nm and 10 nm) PTCDI-C<sub>13</sub>H<sub>27</sub> layers are also plotted. These spectra are scaled with the same factor used for the normalized 50-nm thick PTCDI-C<sub>13</sub>H<sub>27</sub> film spectrum in order to preserve the relative absorbance between the different samples. From Fig. 3.12 it is clear that the overlap with the Alq<sub>3</sub>:DCM<sub>2</sub> light-emitting layer is significantly reduced when thin layers of PTCDI-C<sub>13</sub>H<sub>27</sub> are used, indicating a reduction of photon re-absorption.

To confirm this hypothesis, we have fabricated and characterized an OLED with field-effect-assisted electron transport comprising an ultra-thin 10-nm electron-transporting PTCDI-C<sub>13</sub>H<sub>27</sub> layer. Characterization was performed in an inert N<sub>2</sub> atmosphere immediately after evaporation of the metallic top contact. The experimentally measured characteristics are shown in Fig. 3.13. The device had a width of 1 mm and the metallic cathode was displaced by 1.7  $\mu\text{m}$  with respect to the insulator edge. An  $\eta_{ext}$  of 0.05% was calculated. This is more than two times larger than the value obtained when 50 nm PTCDI-C<sub>13</sub>H<sub>27</sub> was used as the electron-transporting

**Fig. 3.13** Experimentally measured characteristics of a 1 mm wide device, having a distance of 1.7  $\mu\text{m}$  between the metallic top contact and the insulator edge. In this device 10 nm of PTCDI- $\text{C}_{13}\text{H}_{27}$  was used as the electron-transporting layer. (a) Current-voltage characteristics on a logarithmic scale (*dashed line*) and a linear scale (*full line*), and (b)  $\eta_{\text{ext}}$  as a function of the current. (© Wiley-VCH Verlag GmbH & Co. KGaA. Reproduced with permission)



material. From these measurements we infer that re-absorption of emitted photons by PTCDI- $\text{C}_{13}\text{H}_{27}$  is indeed limiting the device performance.

The results above clearly indicate that in order to further improve the device performance other electron-transporting materials should be used. Apart from a high electron field-effect mobility and a slightly lower LUMO than the LUMO of  $\text{Alq}_3$  and  $\text{DCM}_2$ , the material should also have low absorption in the device light-emitting wavelengths, in this case the red spectral region.

### 3.5 Summary and Conclusions

In this chapter, an organic light-emitting diode with field-effect electron transport was proposed as a new device concept complementary to the list of existing electroluminescent devices. In this device configuration, the metallic top contact is remote from the light-emission zone. A micrometer-sized distance between the cathode and the light-emission zone is bridged by electrons with an enhanced field-effect mobility. The light-emission occurs at a fixed position irrespective of the applied bias. We fabricated the device using  $\text{Alq}_3:\text{DCM}_2$  as host-guest light-emitting material system, PTCDI- $\text{C}_{13}\text{H}_{27}$  as electron-transporting material and PTAA as hole-transporting material. Light-emission was found to correlate with the current, and could be modulated by the anode-to-cathode voltage. The measured device operation was confirmed by 2D numerical simulations and by the characteristics of a number of control devices. Devices with smaller distance between the cathode and the insulator edge allowed larger currents at the maximum operating voltage, and

therefore also higher brightness.  $\eta_{ext}$  was confirmed to be as high as in a conventional OLED using the same materials. An increase of  $\eta_{ext}$  could be obtained by decreasing the PTCDI-C<sub>13</sub>H<sub>27</sub> layer thickness, indicating that re-absorption of emitted photons by PTCDI-C<sub>13</sub>H<sub>27</sub> is limiting the device performance. Additional optimization of material combinations may further increase  $\eta_{ext}$ . The quantum efficiency was remarkably constant up to the maximum current, which corresponds to a hole current density in the order of 10 A/cm<sup>2</sup>. This high current density, in combination with reduced optical absorption losses thanks to the remoteness of the metal cathode, may lead to interesting applications as waveguide OLEDs and possibly a laser structure.